Detection of architectural distortion in last screening mammograms prior to detection of breast cancer

Shormistha Prajna

April 11, 2007

1   Introduction

Breast cancer is one of the most important malignancies in women. Statistics from the National Cancer Institute of Canada show that the lifetime probability of a woman developing breast cancer is one in 8.9, with a lifetime probability of one in 27 of dying due to the disease [1]. Since only localized cancer is deemed to be treatable and curable, as opposed to metastasized cancer, early detection of breast cancer is of utmost importance [2].

Mammography is the best available tool for early detection of breast cancer. However, the sensitivity of the screening mammography is influenced by the image quality and the radiologists level of expertise. Contrary to masses and calcifications, the presence of architectural distortion is usually not accompanied by a site of increased density in mammograms. The detection of architectural detection is performed by a radiologist through the identification of more subtle signs of abnormality, such as the presence of spiculations and the distortion of the normal oriented texture pattern of the breast.

Bird et al. [3] observed that, misinterpretation of breast cancer signs accounts for 52% of the errors and overlooking signs is responsible for 43% of the missed lesions. The extent of

errors due to overlooking of lesions reinforces the need for computer-aided diagnosis (CAD) tools in mammography. The clinical significance of early architectural distortion detection is well recognized.Various Computer aided diagnosis (CAD) techniques and systems have been proposed to enhance the sensitivity of the detection of breast cancer.Although these techniques are effective in detecting masses and calcifications, they have failed in detecting architectural distortion with sufficient level of accuracy. Therefore, new system for the detection of architectural distortion should be targeted.

The purpose of this project was to explore the application of fractal analysis and Haralick's texture measure to the investigation of architectural distortion in screening mammograms. The fractal dimension of mammographic regions of interest (ROIs) was calculated using the circular average power spectrum technique. Overall, the average fractal dimension of the normal ROIs was statistically significantly lower than that of the ROIs with architectural distortion. For the first prior year of cancer detection cases, the best receiver operating characteristics (ROC) performance achieved was 0.7357 with the fractal analysis and 0.6962 with Haralick's texture measure.

1.1   Architectural Distortion

Architectural distortion is defined in BI-RADS [4] as follows: "The normal architecture (of the breast) is distorted with no definite mass visible. This includes spiculations radiating from a point and focal retraction or distortion at the edge of the parenchyma. Architectural distortion can also be an associated finding." Focal retraction is considered to be easier to perceive than spiculated distortion within the breast parenchyma [5]. Architectural distortion could be categorized as malignant or benign, the former including cancer and the latter including scar and soft-tissue damage due to trauma.

Architectural distortion is the third most common mammographic sign of non palpable breast cancer [6] but due to its subtlety and variable presentation it is often missed during screening. Specifically, architectural distortion accounts for 12% to 45% of breast cancers

overlooked or misinterpreted at screening mammography [7] [8].

The clinical significance of early architectural distortion detection is well recognized. Burrrell et al. [9], in a study of screening interval breast cancers, showed that architectural distortion is the most commonly missed abnormality in false-negative cases. Broeders et al. [10] suggested that improvement in the detection of architectural distortion could lead to an effective improvement in the prognosis of breast cancer patients.

Several studies have been reported on the detection of architectural distortion. Ayres and Rangayyan applied phase portrait maps to characterize oriented texture patterns of the architectural distortion [11] [12] [13]. Guo et al. [14] investigated the characterization of architectural distortion using the Hausdorff fractal dimension, and a support vector machine classifier to distinguish between ROIs exhibiting architectural distortion and those with normal mammographic patterns. Tourassi et al. [15] studied the use of fractal dimension to differentiate between normal and architectural distortion patterns in mammographic ROIs. Matsubara et al. [16] [17] [18] used mathematical morphology to detect architectural distortion around the skin line and a concentration index to detect architectural distortion within the mammary gland. There are also a number of studies on the performance of commercial CAD system in the detection of architectural distortion.

2 Background

Ayres and Rangayyan [13] have developed techniques for the detection of AD in mammograms, based on the analysis of oriented texture through the application of Gabor filters and linear phase portrait model.The breast contains several piecewise linear structures, such as ligaments, ducts, and blood vessels, that cause directionally oriented texture in mammograms.The presence of AD changes the normal oriented texture of the breast. Characterization of such subtle changes from a pattern recognition perspective was the goal of their work [12].

3

Their overall method for the detection of architectural distortion consists of the following stages:Orientation field extraction using Gabor filters, Curve Linear Structure (CLS) selection, orientation field filtering and down sampling, phase portrait modeling and detection of sites of architectural detection. The orientation field was extracted using a bank of real Gabor filters employed as line detectors. The CLS of interest (spicules and fibrous tissue) were separated from confounding structures (pectoral muscle edge, parenchymal tissue edges, breast boundary, and noise) using the orientation field, the gradient field and a non maximal suppression (NMS) technique. The selected core CLS pixels and the orientation field are filtered and down sampled, to reduce noise and also to reduce the computational effort required by the subsequent methods. The down sampled orientation field was analyzed using phase portraits, yielding three phase portrait maps: node, saddle and spiral. The node map was further analyzed in order to detect the sites of architectural distortion.

The methods were tested with one set of 19 cases of architectural distortion and 41 normal mammograms, and another set of 37 cases of architectural distortion. The resulting free-response receiver operating characteristics (FROC) curve gave the sensitivity rates of 84% at 4.5 false positives per image and 81% at 10 false positives per image for the two sets of images [11].

So further improvement of this technique is required to reduce the number of false positives. In order to reduce the false positive rate in this method, I have proposed an application of fractal analysis and Haralick's 14 texture measure in their method. For this project, 38 mammographic images (14 images from the year of cancer detection, 10 images from first prior year of detection and 10 images from second prior year of detection) of 7 subjects have been used.

3 Materials and methods

3.1 Fractal Analysis

Fractal analysis has become popular in biomedicine as increasingly more studies suggest that it can provide insights into many complex physical phenomena. Often, seemingly irregular structures demonstrate the salient property of self-similarity: to appear similar under a range of measurement scales [19].Consequently, such objects are described by fractal geometry using a non-integer dimension known as the fractal dimension. Generally, the fractal dimension describes the rate of additional structural details as the measurement scale changes.

For digitized images in particular, self-similarity appears to hold in many biomedical systems. For digitized images in particular, self-similarity is satisfied on average and is often limited to a small range of scales. Regardless, fractal analysis has found widespread application in many medical imaging modalities such as radiography, nuclear medicine, CT and MRI. Specifically in mammography, several studies have suggested that the normal breast parenchyma behaves as a fractal object. Tourassi et al. [15] calculated FD of mammographic region of interest (ROIs) using the circular average power spectrum technique. They observed that the presence of architectural distortion disrupts the self-similarity properties and thus alter the fractal dimension of normal breast parenchyma.

Although there are many fractal measures, fractal dimension is the most frequently used in medical imaging. There are a wide variety of techniques available to estimate the fractal dimension of an image. All techniques follow the same underlying principle. An image characteristic is expressed as a function of the scale parameter according to which it is measured. When plotted in the log-log domain, the function is linear. The slope of the fitted line computed by linear regression is linearly related to the fractal dimension of the image. The fractal dimension estimation techniques typically differ in the definition of the scale parameter and the measured image characteristic. Consequently, they produce widely different fractal dimension estimates, often capturing different textural image properties.

In diagnostic imaging the power spectrum estimation method has gained much attention because it appears to provide the most accurate and robust estimates [20] [21]. Aguilar et al. [20] proposed a new frequency analysis method, fractal analysis by circular average (FACA), and an image replication procedure together produce accurate measurements of the fractal dimension of surfaces and profiles, eliminating Fourier transform artifacts which arise from the lack of periodic continuity in real surfaces and profiles.

Schepers et al. [22] examined four methods to estimate the fractal dimension from self-affine signals. The first of these was the relative dispersion (RD) analysis. The others were correlation analysis, rescaled range analysis, and power spectral analysis. The signals analyzed by them were the examples of Brownian noises; they were characterized by a specific power spectrum of the form $S(f)\alpha f^{-\beta}$ where f was frequency. Thus they used the Fourier analysis as their fourth procedure to estimate the fractal dimension. They added that the $1/f$ noise, as it is frequently called, is common in nature, although the physical reason is not well understood. Bak et al. [23] proposed a general model for systems with a very high number of degrees of freedom, called "self-organized criticality", which accounts for both 1/f noise and fractals.

Many physical and biological systems have $1/f^{\beta}$ Fourier spectra - a fractal attribute implying multiple similar mechanisms operating at various spatial and temporal scales. Billock et al. [24] showed that measures of a changing visual environment and perceptual measures of how we see it exhibit fractal-like multiscale characteristics; both dynamic images of natural scenes and human temporal frequency perception display commensurate $1/f^{\beta}$ spectral behavior.

Noise with a power spectral density that varies as an inverse power of frequency is called $1/f^{\beta}$ noise. $1/f^{\beta}$ noise occurs in an impressive variety of physical systems, and numerous complex theories have been proposed to explain it. Lowen et al. [25] constructed two relatively simple renewal processes whose power spectral densities vary as $1/f^{\beta}$. Rios et al. [26] proposed a simple model, able to implement some of the current and most accepted

ideas on $1/f^\beta$ noise and to show a clear $1/f^\beta$ behavior independent on the dimension of the system. They unveiled that the origin of $1/f^\beta$ behavior has to be found in the superposition of power spectra with characteristic frequencies f_c suitably distributed in space.

3.2   Haralick's Measures of Texture

The most commonly used measures of texture, in particular of random texture, are the statistical measures proposed by Haralick et al. [27] [28]. Haralick's measures are based upon the moments of a joint PDF that is estimated as the joint occurrence or co-occurrence of gray levels, known as the gray-level co-occurrence matrix (GCM). GCM are also known as spatial gray-level dependence (SGLD) matrices, and may be computed for various orientations and distances [29].

The GCM $P_{(d,\theta)}(l_1, l_2)$ represents the probability of the pair of gray levels (l_1, l_2) separated by a given distance d at an angle θ. GCMs are constructed by mapping the gray-level co-occurrence counts or probabilities based on the spatial relations of pixels at different angular directions (specified by θ) while scanning the image from left-to-right and top-to-bottom. Due to the fact that neighboring pixels in natural images tend to have nearly the same values, GCMs tend to have large values along and around the main diagonal, and low values away from the diagonal.

Based upon normalized GCMs, Haralick et al. [27] [28] proposed several quantities as measure of texture. The 14 texture measures are : The energy feature, the contrast feature, the correlation measure, the sum of squares, the inverse difference moment, the sum average feature, the sum variance feature, the sum entropy feature, entropy, the difference variance measure, the difference entropy, two information-theoretic measures of correlation and the maximal correlation coefficient feature. Some of the features defined above have values much greater than unity, whereas some of the features have values far less than unity. Normalization to a predefined range, such as [0,1], over the dataset to be analyzed, may be beneficial.

Haralick's measures have been applied for the analysis of texture in several types of images, including medical images.

3.3   Obtaining Data

The project was performed on 38 mammographic images of 7 subjects. They were classified into three categories: 14 images from the year of cancer detection, 10 images from first prior year of detection and 10 images from second prior year of detection. The Ayres-Rangayyan detection method of architectural distortion [11] was applied into all the 38 images. The original resolution of the images was 50 μm/pixel which was down sampled to 200 μm/pixel before applying the Ayres-Rangayyan method.

The whole method consisted of different parts: First the orientation field of the mammographic images were obtained by using a bank of Gabor filters employed as line detectors. Gabor filters were used for the detection of linear patterns and the orientation of local texture. Mammogram exhibit oriented texture due to the presence of normal curvilinear structures (CLS) (such as fibrograndular tissue, vessels and ducts) as well as spicules in the presence of spiculated masses or architectural distortion. The CLS of interest (spicules and fibrous tissue) were separated from confounding structures (edge of the pectoral muscle, parenchymal tissue edges, breast boundary and noise) using the orientation field, the gradient field and the nonmaximal suppression technique. The selected core CLS pixels and the orientation field were filtered and down sampled to an effective resolution of 800 μm/pixel to facilitate efficient phase portrait modeling.

The geometrical patterns in the phase portraits of systems of two, linear, first-order differential equations can be associated with the patterns encountered in an image presenting oriented texture. So the filtered and down sampled orientation field was analyzed through the use of phase portrait. This analysis step produces three maps at the same resolution as that of the down sampled orientation field: a node map,a saddle map and a spiral map. Spiral patterns seldom occur in mammograms and was not included in the present study.

8

The votes for the two types of phase portrait maps: node or saddle were accumulated and analyzed to detect peaks that are related to the sites of architectural distortion. The saddle map was observed to lack discrimination across the mammograms tested, and was eliminated from further consideration. The result of application of the method is illustrated in figure 1 (a). It can be observed that the node map represents a distinct response at the site of architectural distortion. But there are other false positive detections also. After getting the peak indices from the above method, the ROIs surrounding each peak indices were cut out from each of the 38 images. Figure 1 (b) shows an mammogram depicting all the ROIs centering the peak indices. The red rectangle in both the images shows the actual area of architectural distortion. The resolution of the node map is 800 μm/pixel and that of the breast image is 200 μm/pixel. The actual area of architectural distortion was pointed out by a radiologist for all the 38 images.

3.4   Study Design

After getting all the ROIs from the Ayres-Rangayyan method, the circular average power spectrum technique was applied to estimate the fractal dimension [15]. From the three sets of images, 1062 ROIs were obtained. Figure 2 shows some of the 128 x 128 pixel ROIs selected randomly from the 1062 ROIs. Table 1 represents the three data sets with total number of images and selected ROIs.

Data set	No of Images	No of ROIs
Year of Detection	14	398
First Prior Year of detection	14	386
Second Prior Year of Detection	10	278
Total	38	1062

Table 1: No of images and ROIs in each data set

The steps of the circular average power spectrum method are outlined in figure 3. The example image is a 128 x 128 pixel mammographic region (figure 3(a)) . Initially, the two-dimensional power spectrum of the image was obtained using zero padding and a carefully
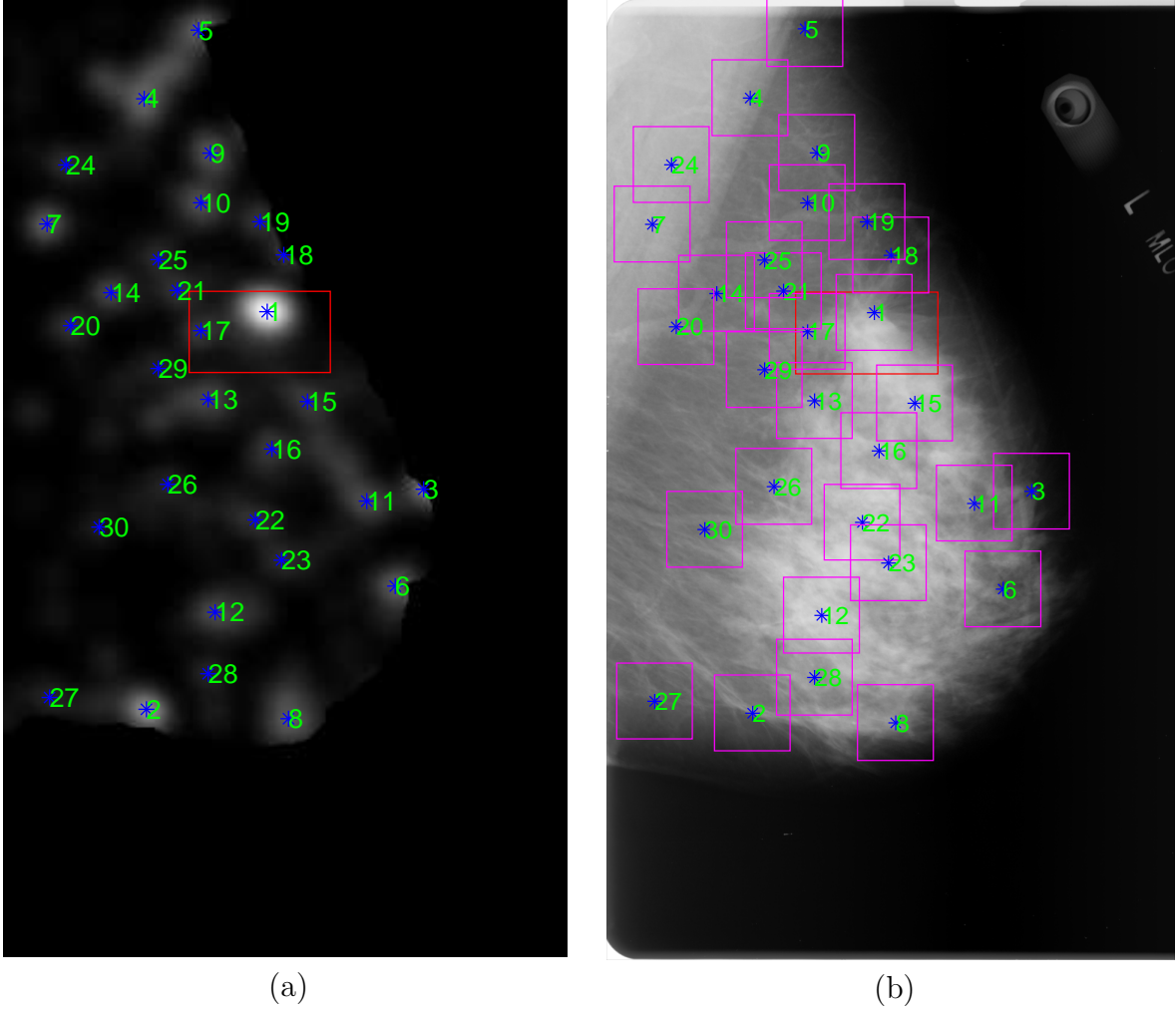
Figure 1: (a)The node map of a left breast image, the blue star (*) sign corresponds to each peak position and the number corresponding to each peak position represents the strongest peak in descending order; (b) The mammogram of a left breast showing the ROIs centering each peak in the image. Size of each ROI is 128 X 128 pixels.

selected window function to ensure better estimation of the power spectrum (figure 3(c)). For this application, I applied a radial Hanning window suggested before in power spectral analysis of mammograms due to the low angular dependence of the mammographic spectrum. Then the 2D power spectrum was transformed into one dimension by linear averaging the spectrum as a function of the radial distance from the zero frequency. The 1D power spectrum $P(f)$ represents the average value in the 2D power spectrum for a given radial distance from the origin or middle of the 2D matrix. The 1D Fourier power spectrum $P(f)$ is related to
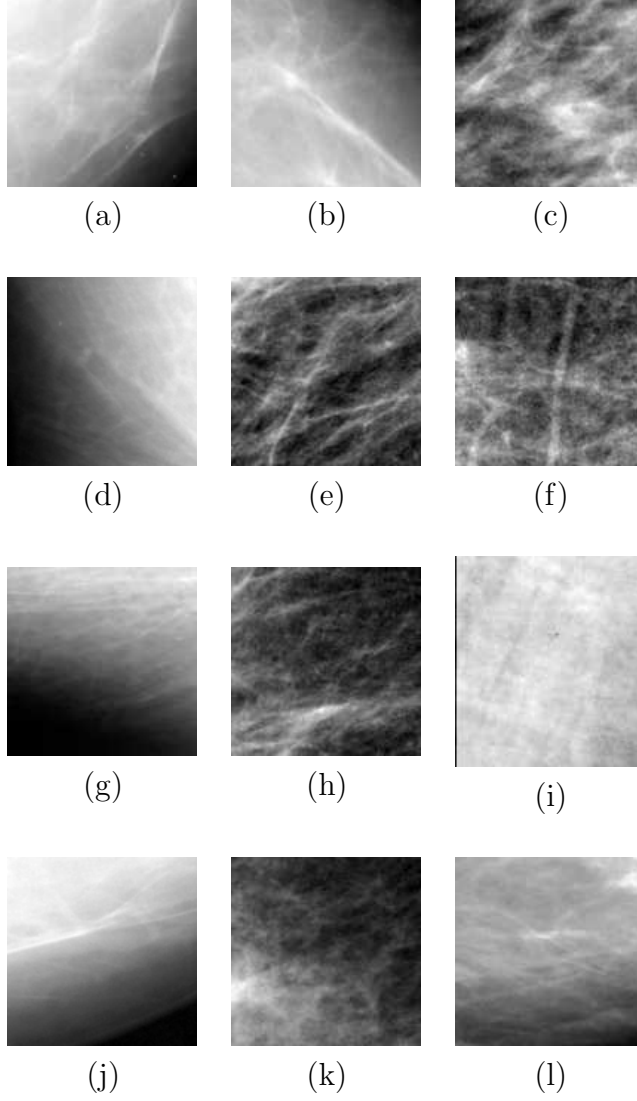
Figure 2: Examples of ROIs

the frequency f by the following equation:

$$P(f) \, \alpha \left(\frac{1}{f}\right)^{\beta} \tag{1}$$

Finally the 1D Fourier power spectrum was plotted on a log-log scale as a function of the frequency (figure 3(d)). Linear regression was applied on the whole frequency range (excluding the low and high frequency of the spectrum) on the log-log plot to estimate the slope β of the fitted line. The estimated slope is linearly related to the fractal dimension of
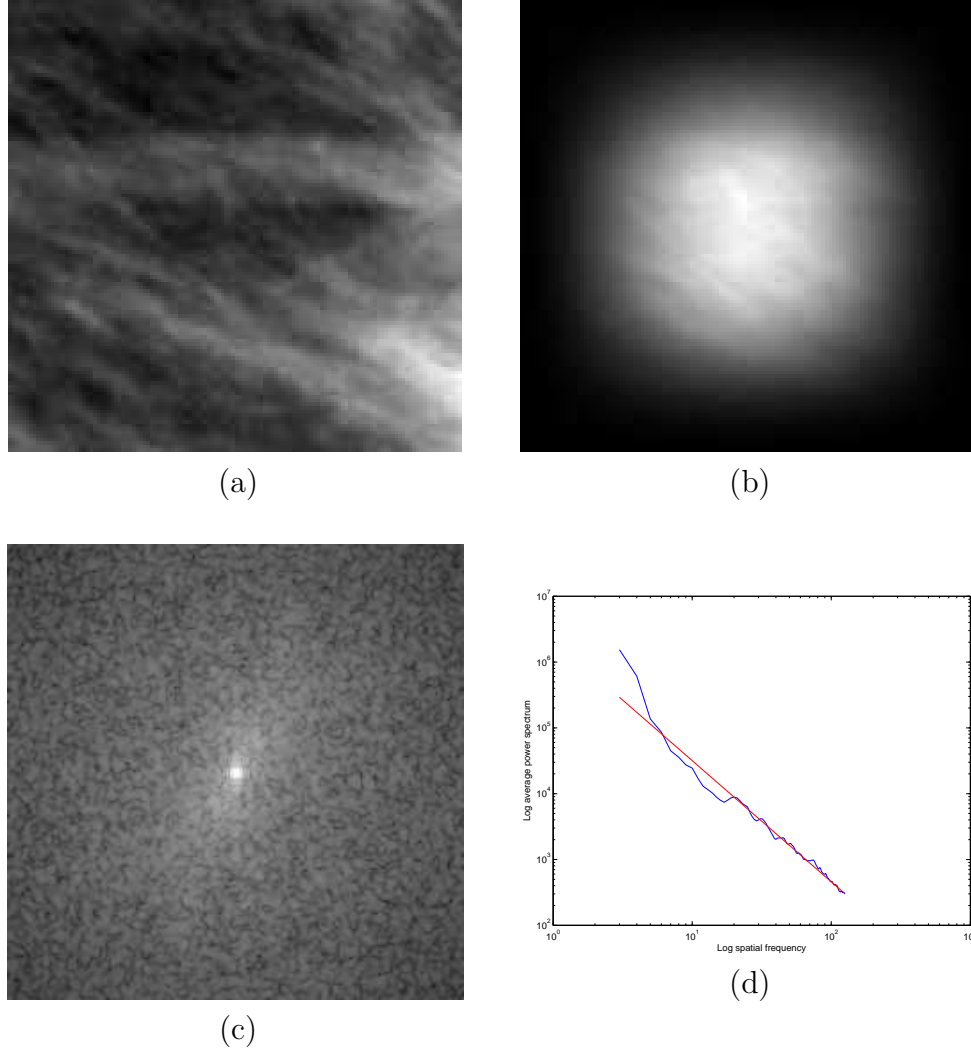
Figure 3: (a) A 128 x 128 pixel mammographic region; (b) The result of applying a radial hanning window to the image of (a); (c) The 2D Fourier spectrum after zero padding the ROI in (b), zero padded ROI is 256 x 256 pixel; (d) The circular averaged 1D Fourier spectrum plotted on a log-log scale a a function of the spatial frequency. The linear fit is also shown with the calculated fractal dimension (FD = 3.0795)

the image [20]:

$$FD = \frac{8 - \beta}{2} \qquad (2)$$

Then the estimated fractal dimension was evaluated using single feature ROC analysis to determine if it can discriminate ROIs depicting normal breast parenchyma. The effect of

ROI size and image resolution was studied in detail. Two different ROI size of 128 x 128 pixels and 64 x 64 pixels were observed at the resolution of 200 μm/pixel. The experiment was also conducted using 50 μm/pixel resolution image with ROI of 256 x 256 pixels.

After obtaining the fractal dimension, the Haralick's 14 texture measures were computed for all the 1062 ROIs of three different sets. For this measure, ROI of 128 x 128 pixels were used at the resolution of 200 μm/pixel. In order to compute Haralick's texture measure, at first the gray-level co-occurrence matrix (GCM) was obtained. Based on the normalized GCM, the 14 different statistical measures were obtained. Then the texture measures were evaluated using ROC analysis. A fisher linear discriminant classifier was used.

4   Results

Since previous studies demonstrated that fractal analysis captures differences in the normal breast parenchyma structure, it is important to quantify how much variability should be expected in the data set for the normal breast parenchyma with architectural distortion. The whole experiment was performed for three different sets of data with total 38 images of 7 subjects. The three categories are: 14 images from the year of cancer detection, 10 images from first prior year of detection and 10 images from second prior year of detection. The fractal analysis was performed on all the three cases. Two different ROI size of 128 x 128 pixels and 64 x 64 pixels were used at the resolution of 200 μm/pixel. The experiment was also conducted using 50 μm/pixel resolution image with ROI of 256 x 256 pixels. Table 2 and table 3 show the average fractal dimension and the standard deviation of the value for both the true positive and false positive cases of 128 x 128 pixel ROI and 64 x 64 pixel ROI respectively. Table 4 shows the data for the 50 μm/pixel resolution image with ROI 256 x 256 pixel. The tables also represent the normalized distance between the means of the true positive and false positive ROIs. The normalized distance between the means of the true positive and false positive ROIs are defined as:

$$d_n = \frac{|m_1 - m_2|}{\sigma_1 + \sigma_2} \tag{3}$$

where m_1 and m_2 are the mean and σ_1 and σ_2 are the standard deviation of fractal dimension value of the true positive and false positive ROIs respectively. The measure d_n provides an indicator of the statistical separability of the PDFs. A limitation of d_n, however, is that $d_n = 0$ if $m_1 = m_2$ regardless of σ_1 and σ_2.

Data Set	True Positive		False Positive		
	Mean	Standard Deviation	Mean	Standard Deviation	Normalized Distance
Year of Detection	3.0558	0.0428	3.0848	0.0617	0.2776
First Prior Year of Detection	3.0421	0.0261	3.0741	0.0521	0.4088
Second prior Year of Detection	3.0495	0.0396	3.0553	0.0612	0.0576

Table 2: Mean, standard deviation and normalized distance of fractal dimension for ROI 128 x 128 pixel at 200 μm/pixel resolution

Data Set	True Positive		False Positive		
	Mean	Standard Deviation	Mean	Standard Deviation	Normalized Distance
Year of Detection	2.9169	0.038	2.9376	0.0632	0.2045
First Prior Year of Detection	2.9029	0.0374	2.924	0.0595	0.2176
Second prior Year of Detection	2.9014	0.0403	2.8948	0.0789	0.0555

Table 3: Mean, standard deviation and normalized distance of fractal dimension for ROI 64 x 64 pixel at 200 μm/pixel resolution

The results shows that overall, the average fractal dimension of the normal ROIs were statistically significantly lower than that of the ROIs with architectural distortion. This result was consistent across almost all the data sets studied with 200 μm/pixel. This opposes the result obtained by Tourassi et al. [15]. They observed that the average fractal dimension of the normal ROIs were statistically significantly higher than that of the ROIs with architectural distortion using resolution of 50 μm/pixel. So in order to compare, the

Data Set	True Positive		False Positive		
	Mean	Standard Deviation	Mean	Standard Deviation	Normalized Distance
Year of Detection	3.3416	0.0354	3.3456	0.0671	0.0391
First Prior Year of Detection	3.3450	0.0379	3.3357	0.0639	0.0919
Second prior Year of Detection	3.3508	0.0329	3.3486	0.0723	0.0176

Table 4: Mean, standard deviation and normalized distance of fractal dimension for ROI 256 x 256 pixel at 50 μm/pixel resolution

experiment was also done at 50 μm/pixel. But at this resolution the result was not significantly distinguishable between the normal ROIs and the ROIs with architectural distortion. The difference of the results from that of Tourassi et al. [15] might have occurred due to several reasons. In their experiment they used the original image of 50 μm/pixel resolution and they selected their normal ROIs randomly from the data set. But for this project, the ROIs were obtained after phase portrait modeling and detection of peak points of probable architectural distortion areas. The peak locations were further used to cut out the ROIs from breast image. Although for a given set of data a constant ROI size was used (for example 128 x 128 pixel), for some of the peak locations which were situated at the edge of the breast, the ROI size was smaller than the defined one. Tourassi et al. [15] applied the zeropadding and radial Hanning window to the ROIs respectively. But for the present project, at first the radial Hanning window was applied to the ROIs and then it was zeropadded while performing the 2D Fourier transform. Furthermore, the normal ROIs used for the experiments had ducts and vessels present in the images which might have not been included in the ROIs those they had selected. Moreover, they applied linear regression on the whole frequency range except the DC component of the spectrum. Here I applied linear regression without considering the low and high frequency range. Because the high and low frequency range of the power spectrum may lead to biased estimates of the parameter β.

Afterward, the estimated fractal dimension was evaluated using single feature ROC analysis. For a resolution of 200 μm/pixel and with 128 x 128 pixel ROI, the best ROC perfor-

mance achieved was 0.7357 for the first prior year of detection cases. The ROC curve for this set of data is shown in figure 4(a).
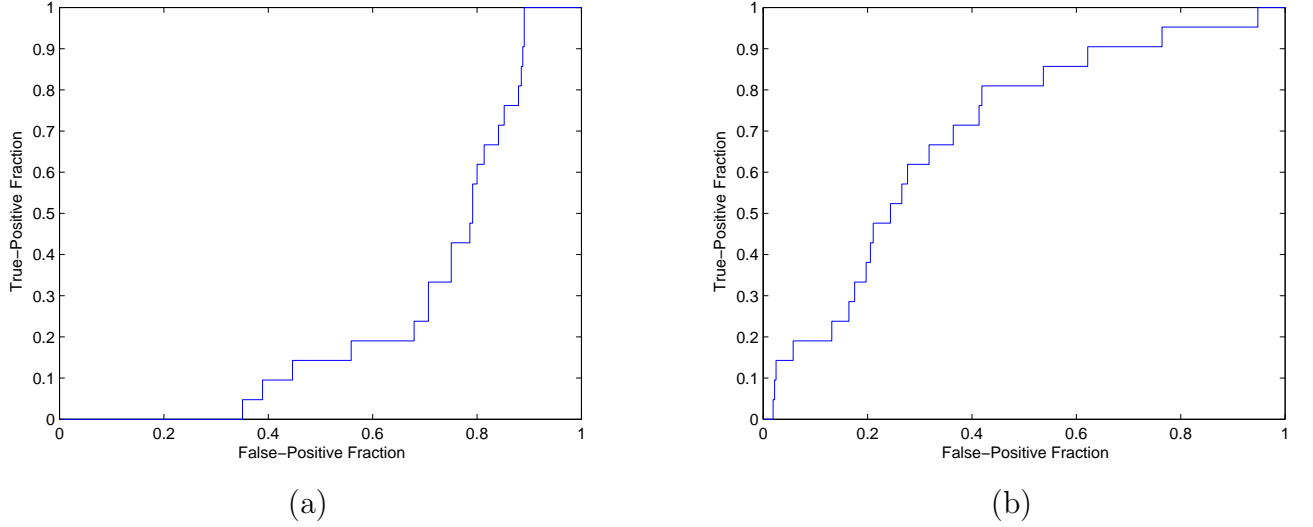

Figure 4: The ROC curve for the first prior year of detection at 200 μm/pixel with ROI of 128 x 128 pixel (a) Result of fractal analysis, $A_z = 0.7357$ (b) Result of Haralick's Texture measure, $A_z = 0.6962$

Haralick's texture measure was also applied on the three sets of data. The performance was evaluated using ROC analysis. A fisher linear discriminant classifier was used. Figure 4(b) shows the ROC curve for the cases of first prior year of detection. Table 5 and 6 represent the area of the ROC curve for different cases of fractal analysis and Haralick's texture measure. It is seen from these tables that for the first prior year of cancer detection cases, ROC performance achieved was 0.7357 with the fractal analysis and 0.6962 with Haralick's texture measure. These results suggest that monitoring the relative change of the fractal dimension across mammographic image could be a promising strategy for architectural distortion.

	A_z at 200 μm/pixel		A_z at 50 μm/pixel
Data Set	ROI 64 x 64 pixel	ROI 128 x 128 pixel	ROI 256 x 256 pixel
Year of Detection	0.6354	0.68	0.5604
First Prior Year of Detection	0.6673	0.7357	0.5238
Second prior Year of Detection	0.5367	0.5381	0.5192

Table 5: The area under ROC curve for different cases of fractal analysis

Data Set	Area of ROC curve
Year of Detection	0.7341
First Prior Year of Detection	0.6962
Second prior Year of Detection	0.6542

Table 6: The area under ROC curve for different cases of Haralick's texture features at 200 μm/pixel with 128 x 128 pixel ROI

5   Discussion

Fractal analysis of mammograms has received attention mainly for two tasks: breast parenchymal density assessment and the diagnostic characterization of calcifications and masses. In this project, I have explored the feasibility of applying the fractal analysis for the auto mated detection of architectural distortion, an understudied yet highly malignant breast abnormality. Since there are a wide range of methods to estimate the fractal dimension of an image (each capturing different image properties), it is noted that any conclusions drawn are relevant to the specific power spectrum estimation method employed in this study.

Since normal breast parenchyma is known to display fractal properties, the study tested if the fractal dimension could discriminate mammographic areas with architectural distortion from those depicting normal breast parenchyma. Architectural distortion as such is not a mass but rather a local disruption of the normal breast tissue pattern. This study demonstrated that the presence of architectural distortion disrupts the statistical properties of the normal breast parenchymal structure, resulting in a higher fractal dimension.

For the project, three different sets with 1062 ROIs were used. From, the ROC analysis it

was found that the cases of first prior year of detection showed significantly good performance of $A_z = 0.7357$ at 200 μm/pixel with 128 x 128 pixel ROI. Though the result of the cases with second prior year of detection was not that significant. The performance was also affected by the image resolution. The images at 200 μm/pixel resolution gave the best results. Furthermore, the performance result was compared with Haralick's texture measure. An area of $A_z = 0.6962$ was found at 200 μm/pixel with 128 x 128 pixel ROI. The Haralick's measure gave significantly good performance of $A_z = 0.6542$ for the cases of second prior year of detection than the fractal analysis where area of ROC curve was found $A_z = 0.5381$.

6 Conclusion

Fractal dimension measurement on digitized mammograms appear to be a promising way to assess locally the presence of architectural distortion. The present study was a continuation of the Ayres-Rangayyan [11] technique. The goal was to reduce the number of false positive detection. The aspect of applying the fractal analysis using circular average power spectrum technique and Haralick's texture measure in reducing the number of false positives was studied. And the study gave quite promising results for future implementation. So, in future I would like to observe the performance of fractal dimension and Haralick's features together to obtain the ROC curve. Other texture measures like Law's texture measure can also be included in the features. In order to compare the results of Ayres-Rangayyan method with my study, I would also like to perform the free-response receiver operating characteristics (FROC) analysis. Thus development of CAD techniques dedicated to the detection and localization of architectural distortion should lead to efficient detection of early signs of breast cancer.

References

[1] National Cancer Institute of Canada. Canadian cancer statistics 2006, 2006.

[2] M. A. Schneider. Better detection: Improving our chances. In M. J. Yaffe, editor, *Digital Mammography: 5th International Workshop on Digital Mammography*, pages 3–6, Toronto, ON, Canada, June 2000. Medical Physics Publishing.

[3] R. E. Bird, T. W. Wallace, and B. C. Yankaskas. Analysis of cancers missed at screening mammography. *Radiology*, 184(3):613–617, 1992.

[4] American College of Radiology (ACR). *Illustrated Breast Imaging Reporting and Data System (BI-RADS)*. American College of Radiology, Reston, VA, 3rd edition, 1998.

[5] M. J. Homer. *Mammographic Interpretation: A Practical Approach*. McGraw-Hill, New York, NY, 2nd edition, 1997.

[6] A. M. Knutzen and J. J. Gisvold. Likelihood of malignant disease for various categories of mammographically detected, nonpalpable breast lesions. *Mayo Clinic Proceedings*, 68:454–460, 1993.

[7] B. C. Yankaskas, M. J. Schell, R. E. Bird, and D. A. Desrochers. Reassesment of breast cancers missed during routine screening mammography: a community based study. *American Journal of Roentgenology*, 177:535–541, 2001.

[8] H. Burrell, A. Evans, A. Wilson, and S. Pinder. False-negative breast screening assesment: what lessons we can learn? *Clinical Radiology*, 56:385–388, 2001.

[9] H. C. Burrell, D. M. Sibbering, A. R. M. Wilson, S. E. Pinder, A. J. Evans, L. J. Yeoman, C. W. Elston, I. O. Ellis, R. W. Blamey, and J. F. R. Robertson. Screening interval breast cancers: Mammographic features and prognostic factors. *Radiology*, 199(4):811–817, 1996.

[10] M. J. M. Broeders, N. C. Onland-Moret, H. J. T. M. Rijken, J. H. C. L. Hendriks, A. L. M. Verbeek, and R. Holland. Use of previous screening mammograms to identify features indicating cases that would have a possible gain in prognosis following earlier detection. *European Journal of Cancer*, 39(12):1770–1775, 1993.

[11] R. M. Rangayyan and F. J. Ayres. Detection of architectural distortion in mammograms using a shape-constrained phase portrait model. In H. U. Lemke, K. Inamura, K. Doi, M. W. Vannier, and A. G. Farman, editors, *Proceedings of the 20th International Congress and Exhibition on Computer Assisted Radiology and Surgery (CARS 2006)*, pages 334–336, Osaka, Japan, July 2006. Springer.

[12] R. M. Rangayyan and F. J. Ayres. Gabor filters and phase portraits for the detection of architectural distortion in mammograms. *Medical and Biological Engineering and Computing*, 44:883–894, August 2006.

[13] F. J. Ayres and R. M. Rangayyan. Characterization of architectural distortion in mammograms. *IEEE Engineering in Medicine and Biology Magazine*, 24(1):59–67, January 2005.

[14] Q. Guo, J. Shao, and V. Ruiz. Investigation of support vector machine for the detection of architectural distortion in mammographic images. *Journal of Physics: Conference Series*, 15:88–94, 2005.

[15] G. D. Tourassi, D. M. Delong, and C. E. Floyd Jr. A study on the computerized fractal analysis of architectural distortion in screening mammograms. *Physics in Medicine and Biology*, 51(5):1299–1312, 2006.

[16] T. Matsubara, D. Fukuoka, N. Yagi, T. Hara, H. Fujita, Y. Inenaga, S. Kasai, A. Kano, T. Endo, and T. Iwase. Detection method for architectural distortion based on analysis of structure of mammary gland on mammograms. In *Proceedings of the 19th Interna-*

tional Congress and Exhibition on Computer Assisted Radiology and Surgery (CARS 2005), pages 1036–1040, Berlin, Germany, 2005. Elsevier.

[17] T. Matsubara, T. Ichikawa, T. Hara, H. Fujita, S. Kasai, T. Endo, and T. Iwase. Automated detection methods for architectural distortions around skinline and within mammary gland on mammograms. In H. U. Lemke, M. W. Vannier, K. Inamura, A. G. Farman, K. Doi, and J. H. C. Reiber, editors, *International Congress Series: Proceedings of the 17th International Congress and Exhibition on Computer Assisted Radiology and Surgery*, pages 950–955, London, UK, June 2003. Elsevier.

[18] T. Matsubara, D. Yamazaki, T. Hara, H. Fujita, S. Kasai, T. Endo, and T. Iwase. Automated detection of architectural distortion on mammograms. In H.-O. Peitgen, editor, *Digital Mammography IWDM 2002: 6th International Workshop on Digital Mammography*, pages 350–352, Bremen, Germany, June 2002. Springer-Verlag.

[19] B. B. Mandelbrot. *The Fractal Geometry of Nature*. San Francisco: Freeman, 1983.

[20] M. Aguilar, E. Anguiano, and M. A. Pancorbo. Fractal characterization by frequency analysis: II. A new method. *Journal of Microscopy*, 172:233–238, 1993.

[21] E. Anguiano, M. A. Pancorbo, and M. Aguilar. Fractal characterization by frequency analysis: I. surfaces. *Journal of Microscopy*, 172:223–232, 1993.

[22] Hans E. Schepers, Johannes H. G. M. van Beek, and james B. Bassingthwaighte. Four methods to estimate the fractal dimension from self-affine signals. *IEEE Enginerring in Medicine and Biology Magazine*, 11:57–64, June 1992.

[23] Per Bak, Chao Tang, and Kurt Wiesenfeld. Self-organized criticality: An explanation of 1/f noise. *The American Physical Society*, 59:381–384, 1987.

[24] V. A. Billock, G. C. De Guzman, and J. A. S. Kelso. Fractal time and 1/f spectra in dynamic images and human vision. *Elsevier Science B.V.*, 148:136–146, 2001.

[25] S. B. Lowen and M. C. Teich. Fractal renewal processes generate 1/f noise. *The American Physical Society*, 47:992–1001, 1993.

[26] Paolo De Los Rios and Yi-Cheng Zhang. Universal / noise from dissipative selg-organized criticality models. *The American Physical Society*, 82:472–475, 1999.

[27] R. M. Haralick. Statistical and structural approaches to texture. *Proceedings of the IEEE*, 67:786–804, May 1979.

[28] R. M. Haralick, K. Shanmugam, and I. Dinstein. Textural features for image classification. *IEEE Transactions on Systems, Man, Cybernetics, SMC*, 3(6):610–622, 1973.

[29] R. M. Rangayyan. *Biomedical Image Analysis*. The Biomedical Engineering Series. CRC Press, Boca Raton, FL, 2005.